INVITED PAPER

Polymer optical fiber sensors in human life safety

C. A. F. Marques[1,2], D. J. Webb[2], P. Andre[3]

1 Instituto de Telecomunicações, I3N and Physics Department, University of Aveiro, Campus de Santiago, 3810-193 Aveiro, Portugal
2 Aston Institute of Photonic Technologies, Aston University, Aston Triangle, Birmingham, B7 4ET, United Kingdom
3 Instituto de Telecomunicações and Department of Electrical and Computer Engineering, Instituto Superior Técnico, University of Lisbon, 1049-001 Lisbon, Portugal
*Corresponding author: cmarques@av.it.pt

Abstract

The current state of research into polymer optical fiber (POF) sensors linked to safety in human life is summarized in this paper. This topic is directly related with new solutions for civil aircraft, structural health monitoring, healthcare and biomedicine fields. In the last years, the properties of polymers have been explored to identify situations offering potential advantages over conventional silica fiber sensing technology, replacing, in some cases, problematic electronic technology used in these mentioned fields, where there are some issues to overcome. POFs could preferably replace their silica counterparts, with improved performance and biocompatibility. Finally, new developments are reported which use the unique properties of POF.

1. Introduction

Optical fiber sensors can be used for monitoring temperature, strain, deformation, refractive index and acceleration, among other physical quantities, with advantages over traditional electronic sensors. These sensors present significant advantages very well reported when compared with conventional electromechanical sensors (including piezoelectric transducers, capacitive and ultrasonic devices), especially for medical applications, structural health monitoring, healthcare, among others, due to its high accuracy; robustness; small size and light weight; electrical isolation, making them intrinsically safer than electronic sensors; immunity to electromagnetic interference; being also biocompatible and safe for the human.

For sensing applications both silica optical fiber (SOF) and polymer optical fiber (POF) can be used. SOF sensors are the most studied and applied but POF sensors are emerging as a good alternative, mainly when high flexibility and robustness are required [1]. POF sensors received high attention recently due to their unique properties compared to the conventional SOF sensors [1]. Advantages such as higher flexibility in bending, biocompatibility [2], higher failure strain [3], higher fracture toughness, and lower production cost, are significant for many sensing applications. The lower Young's modulus of POF [4] provides enhanced sensitivity to POF sensors when are used for strain [5], stress and force [6], pressure [7], and acoustic wave detection [8]. There are also some hydrophilic polymeric materials such as poly (methyl methacrylate) (PMMA) that can absorb water, enable them for humidity detection applications [9]. Also, some materials such as TOPAS (cyclic olefin copolymer (COC)) can offer insensitivity to water

which can be useful for biomedical applications [10,11]. The material properties of polymers can be chemically modified by adding other organic compounds to achieve specific desirable characteristics. An example is the perfluorinated POF, commercially known as CYTOP (amorphous fluoropolymer), which the carbon-hydrogen bonds have been replaced with carbon-fluorine bonds to reduce the fiber attenuation [12]. One of the drawbacks of POF is its viscoelastic nature. When cyclic loading is applied to the POF sensor, creep and hysteresis effects are introduced due to the strain and stress phase mismatch [3], which can alter the accuracy of the sensor reading. It is demonstrated that these effects can be reduced by applying thermal treatment in POF sensors [13].

There is a myriad of applications where POF technology is used such as geophysical surveying and security [14,15], groundwater level monitoring [16], water detection in fuel [17], healthcare [18], optoacoustic endoscopic imaging [19], central arterial pressure monitoring [20], on-line remote dosimetry [21], structural health monitoring [22], decubitus prevention [23], among others. As we can observe, all these applications are closely related to human safety.

2. POF materials

In the last years, there was an exponential increasing of research using POF technology from its fabrication procedure to its characterization as a potential sensor for many real applications. Many types of material for POF fabrication were investigated in order to produce the best quality sensors for different requirements in sensing fields. To date, PMMA is the most used material in POF fabrication, although the use of some alternative plastics, such as CYTOP [12,24], TOPAS [10,11,25], and polycarbonate (PC) fibers [26] have recently been investigated. PMMA POFs [1, 3, 5-9,13,16-22, 27-31] present a response of the sensors dependent on both temperature and humidity [27-31]. This fact, together with the issue of high loss and low operating temperature, has been hindering the application of polymer sensors in key strain sensing and biosensing areas [32]. Although progress has been made towards reducing the influence of humidity on PMMA fibers by doping [33], the issue of humidity dependency was first solved with the fabrication of the first TOPAS mPOF in 2007 [34,35]. The significant polymer TOPAS belongs to the class of COCs, which is a class of optical thermoplastics that are chemically inert and have a very low moisture uptake, high water barrier, and good optical transmission [36]. This means that a TOPAS sensor is humidity insensitive [10]. However, the aim with the original fiber was to use the chemical inertness of TOPAS for localized fluorescence-based biosensing [34, 35]. So, the key advantages of the TOPAS fiber are low water absorption, high operating temperature (more than 135^{o}C) and chemical inertness to acids and bases and many polar solvents as compared to the conventional PMMA based POFs [11]. A recent development that has a great potential benefit is the production of sensors in perfluorinated fiber [37], in which the losses are significantly less than in PMMA. PC optical fibers were introduced by Fujitsu in 1986 (the core was made of PC, with a polyolefin-based material as the cladding) [38] and have been extensively studied and used since then [39–41]. Polycarbonate is an engineering plastic that exhibits excellent clarity and impact strength [42]. The main advantage of using this material for optical fiber fabrication indeed lies in the well-balanced combination of its optical and mechanical properties. Firstly, it is transparent to visible light [43] and for this reason it can be considered as a natural alternative to PMMA. Secondly, PC usually yields and breaks at elevated values of strain, and is highly flexible in bending [43]. In addition, its glass transition temperature (Tg) is one of the highest among transparent plastics (145^{o}C), thereby resulting in a larger

available temperature range. These properties make PC fibers particularly attractive for those applications requiring high-temperature-resistant polymer sensors, as long as the specific application does not involve long-term exposure to a high-humidity environment at high temperature. To note that with each material different types of POF are produced, including step-index and microstructured POF (mPOF). Moreover, we can have undoped and doped POFs, with the last one aiming to improve the UV photosensitivity. A detailed control of all stages of the POF production process—polymerization, preforms and fiber drawing – is a crucial point to achieve good POF performance.

3. POF based sensors: latest achievements

These different fabricated POFs can be used as sensors (which can be based on different technologies) to monitor the external environment, for instance on fiber Bragg gratings (FBG) or light intensity modulation [44]. These sensing methods will be briefly discussed, where the particular properties of polymers offer some advantage.

3.1. Fiber Bragg grating based sensors

The development of UV lasers has made possible the inscription of refraction gratings in the core of the optical fibers. An FBG is a periodic modulation of the optical fiber core refractive index. When illuminated by a broadband light source the FBG will reflect selectively the wavelength that satisfies the first order Bragg condition:

$$\lambda_B = 2n_{eff}\Lambda(z) \quad (1)$$

where λ_B is the central reflected Bragg wavelength, n_{eff} is the effective refractive index of the optical fiber core, and Λ is the period of the refractive index modulation on the optical fiber core. In this way, the reflected spectrum of a FBG is a narrow spectral band, peaking at λ_B. From Eq. 1 it is clear that any external parameter that affects the refractive index or the physical modulation of the grating period, such as temperature or strain variations will change the Bragg wavelength. Therefore, this value becomes the parameter to monitor in FBG based sensors because it is related with the variable for which the sensor is sensitive [45]. The main advantages of FBG based sensors besides the general optical fiber sensors advantages already referred, are the multiplexing capabilities and lower visual impact. Differing from the intensity based sensors, FBGs are used for critical measures with higher signal-to-noise ratios need.

The FBG can have several distinct FBG structures such as: uniform Bragg grating, characterized by a constant grating pitch (spacing between grating planes); tilted FBG (TFBG), which has the grating planes tilted with respect to the fiber longitudinal axis; and the chirped Bragg grating (CFBG) that has a non-periodic pitch, usually displaying a linear variation in the grating pitch, designed as chirp [46,47]. There are several works using SOF technology for sensing and data communications [46-49]. In POF technology, the most widely used type in POF sensing applications is the uniform FBG [1,6-11,13,17,24,26-32,37,50]. However, recently some great papers showing TFBGs and CFBG in POF for sensing applications were reported [51,52,53].

TFBGs belong to the short period grating family (grating period close to 500 nm for use in the C+L bands) and possess a refractive index modulation slightly angled with respect to the parallel of the optical fiber

propagation axis. They provide two kinds of couplings: the self-backward coupling of the core mode and numerous backward couplings between the core mode and different cladding modes [48]. TFBGs present comb-like transmitted amplitude spectra composed of several tens of narrow-band resonances (full width at half-maximum (FWHM) ~100 pm). These unique spectral features make possible a wealth of applications [54-57]. Xuehao Hu *et al* investigated the first TFBG photo-inscribed in PMMA POF for (bio)chemical sensing applications [51]. Fig. 1 presents the transmitted amplitude spectra of three TFBGs with tilt angles of 1.5°, 3.0°, and 4.5°, respectively. Conclusions similar to the case of silica TFBGs can be obtained. For higher tilt angles, the spectral content increases thanks to the coupling of higher cladding mode resonances, while the Bragg wavelength is red-shifted and the core mode resonance reflectivity decreases. The reflectivity of the Bragg resonance was measured and its equal to 16% for the 1.5° TFBG, 12% for the 3.0° TFBG and 2% for the 4.5° TFBG. It can also be noticed that the peak-to-peak amplitude of the cladding modes decreases with the tilt angle increasing, in accordance with [48]. The same group reported recently the first excitation of surface plasmon waves at near-infrared wavelengths using weakly TFBGs photo-inscribed in the core of step-index PMMA POFs and the fiber coated with a thin gold layer [52]. The refractometric sensitivity can reach ~550 nm⁄RIU with a figure of merit of more than 2000 and intrinsic temperature self-compensation. This kind of sensor is particularly relevant to in situ operation.

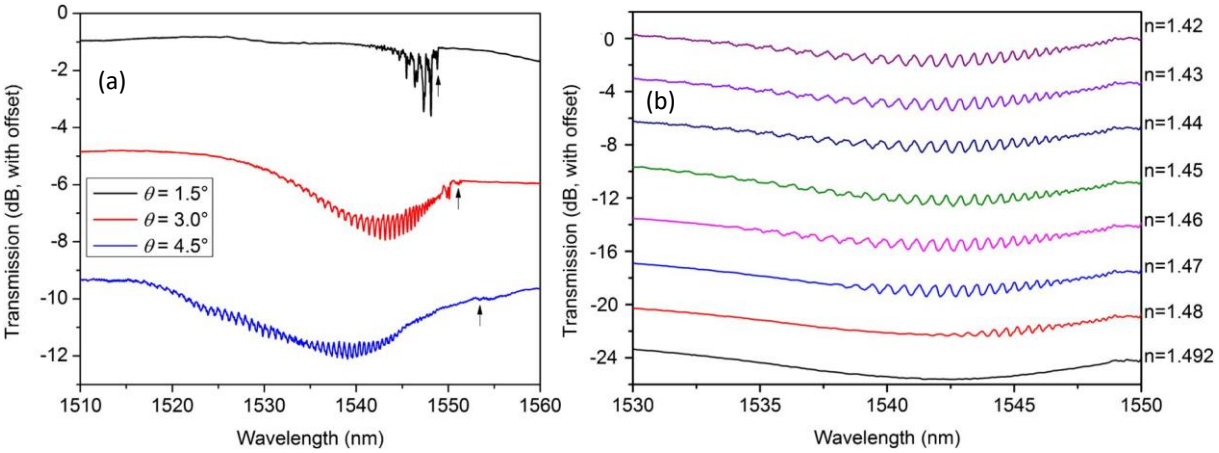

Figure 1. (a) Transmitted amplitude spectra of three TFBGs with tilt angles of 1.5°, 3.0°, and 4.5°. (b) Transmitted amplitude spectrum evolution (vertical scale with offset) as a function of the SRI value in the range 1.42–1.49 [51].

The CFBGs, also called aperiodic Bragg gratings, are known in the literature for gratings with chirp and generally refer to gratings in which the resonance condition varies along its length. If the variation of the periodicity is small, it can be considered locally uniform. Because of this, each part of the grating will reflect different wavelengths without affecting each other [58]. The most common aperiodic FBGs are gratings with variable period along its longitudinal extension. Fig. 2 shows schematically the period variation over an FBG with linear aperiodicity. The modulation period *ʌ(z)* follows a linear profile:

$$\Lambda(z) = \Lambda_0 + kz \tag{2}$$

for *0 < z < L*, where *L* is the grating length; *k* is the chirp coefficient, which defines the increase of refractive index period per unit of length. The period of an aperiodic FBG can be expressed by a *N*

degree polynomial given as $\Lambda(z) = \Lambda_0 + \Lambda_1 z + \ldots + \Lambda_N z^N$, which is important for optical communications field. The aperiodicity has effect in two properties of Bragg gratings: the bandwidth and group delay. In aperiodic FBGs the resonance condition occurs for various wavelengths, resulting in a grating with a bandwidth much higher than conventional FBGs. The group delay characteristics of the grating are different from conventional gratings. Since different wavelengths are reflected in different positions on the fiber, it causes a group delay dependent on the wavelength. This kind of FBGs and analysis are used in optical communications and sensing applications [59-63].

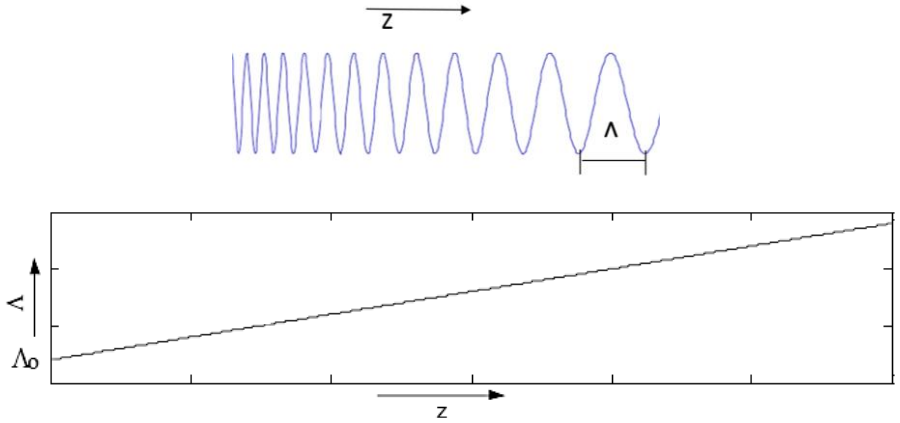

Figure 2. Illustration of the refractive index variation in a linear aperiodic grating (top) and the respective period variation (bottom) [53].

Recently, Marques *et al* investigated the very first CFBG photo-inscribed in POFs [53]. The fast growing achieved (only a few seconds of the UV exposure) is related with the high absorption of the PMMA under 248 nm UV light. The CFBG in POF (CPOFBG) was recorded in the core of an undoped step-index POF and presents a rejection band of more than 16 dB and an FWHM bandwidth of 3.9 nm as shown in Fig. 3. These results pave the way to further developments of CFBGs in POFs (using even TOPAS [11] or polycarbonate fibers [26]) and to their use for different domains, such as biomedicine and SHM (including in aeronautical structures) [59-63] where POFs could preferably replace their silica counterparts, with improved bending tolerance and biocompatibility. Here, we show the first group delay collected from a 25 mm long CFBG photo-inscribed in POF, achieving a dispersion (defined as the rate of change of group delay, τ, with wavelength) of around -66 ps/nm, displayed in Fig. 3. However, the obtained ripple is high and improvements need to be done.

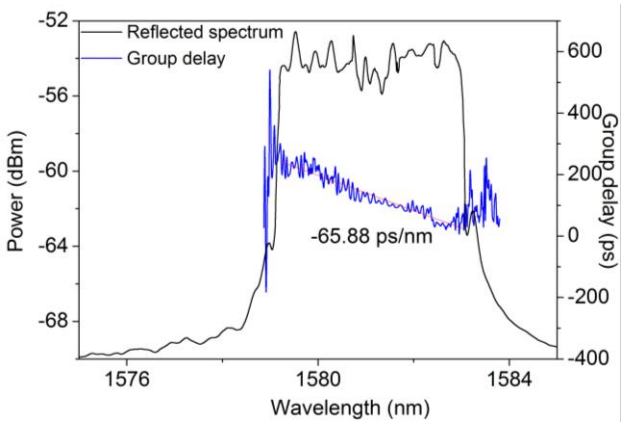

Figure 3. CPOFBG recorded in the core of an undoped step-index POF. Group delay collected from a 25 mm long CFBG photo-inscribed in POF.

3.2. Intensity based optical fiber sensors

Optical fiber sensors based on intensity modulation are probably the simplest in terms of operating principles and instrumentation. As the name specifies, in this approach the sensing variables are detected by changes in the fiber output light intensity. In general, the experimental configurations include a light source, one or more optical fibers and a photodetector or an optical spectrum analyzer. The advantages of this sensing method are its low cost, ease of production and simplicity of signal processing [44].

Leitão *et al* investigated the carotid distension waves acquired with a POF sensor as an alternative to tonometry for central arterial systolic pressure assessment in young subjects [20]. Fig. 4 represents a scheme of the probe working principle. These pre-clinical results support a future clinical validation study in larger and broader cohorts. Also, the same group reported the applicability of both FBG and POF intensity based sensor in assessing the central pressure at different subjects and situations. They found that the FBG probe system has a resolution of around 0.02 µm and the POF system 0.05 µm. It was demonstrated that the low cost POF sensor can be a suitable alternative to traditional methods to assess arterial central pressure. The results from this study shown that the POF system is suitable and meet the requirements for further clinical trials against the traditional equipment's and invasive aortic pressure measurements, in a more diverse sample of subjects.

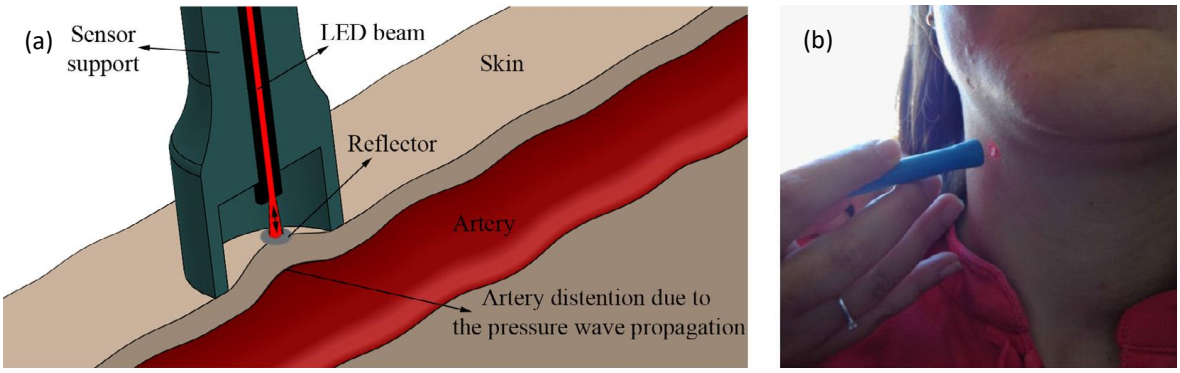

Figure 4. POF device: (a) schematization and (b) photograph of the application on the carotid artery's surface [20].

Mesquita *et al* described the testing and application of a low cost POF sensor on the monitoring of groundwater levels [16]. Fig. 5 shows the experimental setup and details about POF in the mold. The sensors were tested under two experimental setups: water level variation (increasing and decreasing of the water level) and groundwater increase simulation, in a soil column. The analysis of the optical signal's amplitude and its variations due to the increasing or decreasing of water level showed that both tested sensors presented an appropriate performance and adequate sensibility to groundwater level variation and, therefore, can be used for in situ applications of monitoring. The advantages of employing such sensors in structural health monitoring systems to monitor groundwater levels, are the simplicity of the measurement system and a suitable sensitivity, added to the low manufacturing, interrogation and maintenance costs.

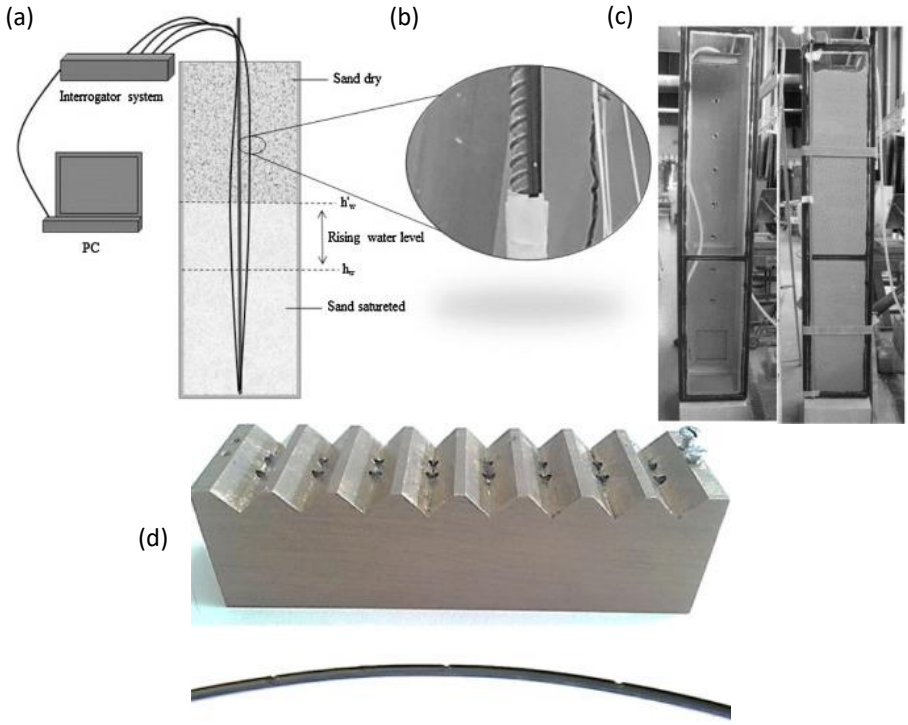

Figure 5. Experimental setup: (a) the experimental implementation and its components; (b) detail of the groove in the fiber during the optical signal processing, and (c) soil test box without sand and with sand. (d) Brass mold used to create the grooves in the POF, and a detail of the POF with the grooves is shown below the mold photograph [16].

Antunes *et al* demonstrated the feasibility of POF based accelerometers for the SHM of civil engineering structures based on measurements of their dynamic response, namely to estimate natural frequencies [22]. A low-cost POF-based accelerometer was used to estimate its natural frequency with a relative error of 0.36%, comparatively to the value estimated recurring to a calibrated electronic sensor. This kind of POF based accelerometers can be used to evaluate the inevitable aging and degradation resulting from operational environments in bridges, buildings, among others.

Scully *et al* developed a range of signal processing methods to extract data from POF sensor elements to measure human motion ranging from balance to walking [18,64]. Together with tomographic and analogue null balance methods, they explored pattern recognition and machine learning classification, to identify different types of walking. Applications include gait analysis for detection of early onset of

dementia affecting the executive function of the brain (and thus mobility), rehabilitation, sports and security, imaging and recording of the geometry, spatial location and time of each footfall in order to extract gait measures that define mobility.

Quandt *et al* investigated the use of new-developed POFs for the development of textile sensors leads to flexible, wearable sensors [23]. These photonic textiles show versatility with sensor placement and the POF fabrics have shown to be low-friction. They can hence be used for long-term measurements, also on sensitive skin. These comfortable monitoring devices will allow an improvement in the quality of life.

Also, Hassan *et al* presented an in-vitro sensing of glucose using a newly developed efficient optical fiber glucose sensor based on a Compound Parabolic Concentrator (CPC) tipped POF [65]. In-vitro measurements for two glucose concentrations (40 and 400 mg/dL) confirmed that the CPC tipped sensors efficiently can detect both glucose concentrations. According to the World Health Organization, diabetes will be the 7th leading cause of death in 2030 [66]. Insulin is a hormone that regulates the blood glucose levels and proper insulin delivery based on continuous glucose monitoring is extremely important for diabetes patients. This requires a low-cost, accurate and bio-compatible sensor, which is easy to operate and can be placed in the patient body for frequent or continuous glucose measurements.

Using these different sensing methods, it is possible to achieve numerous applications based on POF technology in order to obtain from particular properties some advantage that the SOF technology cannot bring with such impact.

4. Latest applications: link with safety of human life

This section is focused in the recent developments and applications proposed for polymer FBG sensors, where the particular properties of polymers offer some advantage in terms of performance compared with SOF technology, and even in terms of safety when compared with conventional technology used so far.

4.1. Polymer FBG sensor for underwater applications

In the subsea environment, the monitoring of acoustic signals and vibration is crucial for different applications such as in geophysical surveying and security, e.g. the detection of unwanted craft or personnel. Current technology is predominantly based on piezoelectric strain sensors but although they have satisfactory performance, they suffer from other limitations: physical size; limited deployment range without local power and amplification; lack of multiplexing capabilities.

To solve these problems, there has been a steady move to introduce optical fiber based systems, firstly for surveillance [14] and for geophysical surveying [15]. The first systems were interferometric in nature, involving coils of fiber wound on a compliant mandrel. Such systems still have the disadvantage of requiring a large diameter cable to contain the coil. Efforts have been made to use Bragg grating sensors along a single straight fiber, but for the most demanding applications standard Bragg gratings do not possess sufficient sensitivity and it has been proven to be necessary the use of fiber laser sensors [67]. However, even though these fiber laser sensors keep the sensor diameter down, they add complexity

and increase the costs. Previous fiber sensor research has focused on SOF solutions and recently they needed to use particular coatings to improve the sensitivity [68] and only now, with the increasing maturity of the polymer, FBG technology have the first relevant but preliminary studies been carried out, for example when looking at an accelerometer, assessing strain response up to a few kHz [69] and demonstrating a fiber grating based acoustic modulator [70].

Here, we present the recent experimental studies on FBG based interferometric scheme for monitoring low-frequency (few kHz) waves using POF in a comparison with the response of SOF. On the other hand, fiber Mach-Zehnder interferometers (MZI) are widely used for FBG sensor interrogation purpose due to their advantages in terms of high resolution, wide bandwidth, and tunable sensitivity. They are appropriate for dynamic strain measurement applications in the areas of vibration analysis, hydrophones, and acoustic emission studies. The interferometer converts the Bragg wavelength shift of an FBG sensor into a corresponding phase shift in an electrical carrier, which can be demodulated using conventional techniques. In this work, a heterodyne technique based on an unbalanced interferometric wavelength discriminator is described and the performance of both types of fiber containing FBGs is compared. A considerable sensitivity improvement is achieved using polymer FBG (around 6 times better), which arises as a result of the much more compliant nature of POF compared to silica fiber (3 GPa and 72 GPa, respectively). Essentially, and despite the strain sensitivity of silica and POFBGs being very similar, this renders the POF much more sensitive to the applied stress resulting from acoustic signals or vibration. Preliminary results give noise-limited pressure resolutions of 3.68×10^{-6} Pa and 1.33×10^{-5} Pa for SOF and POF, respectively, each within a 100 Hz bandwidth.

The arrangement used to interrogate the grating is shown in Fig. 6. It utilized a ramped lithium niobate phase modulator (accurately set to produce a 2π peak-to-peak phase excursion) to frequency shift the light in one arm of an unbalanced MZI and thus allowing the use of heterodyne signal processing [71]. Light from a broadband light source (provided by Thorlabs ASE-FL7002-C4), giving an output power of 20 mW centered at 1560 nm with a bandwidth of 80 nm, was launched into the unbalanced MZI; hence a channelled spectrum was created at the interferometer's outputs that was incident on the grating. Incorporated in one arm of the MZI was the phase modulator. The other arm contained a variable air gap that allowed the optical path difference (OPD) between the two arms to be adjusted. Provided that the OPD between the MZI's arms is longer than the source coherence length and shorter than the effective coherence length of the back-reflected light from the grating, interference signals are observed at the detector, which can be expressed as

$$I\left(\lambda_B\right) = A\left\{1+V\cos\left[\omega_r t+\Phi+\delta\Phi\sin\omega t+\phi\left(t\right)\right]\right\}, \tag{3}$$

where λ_B is the wavelength of the reflected light from the modulated grating, ω_r is the angular frequency of the ramp modulation, ω is the angular strain frequency experienced by the grating, A is proportional to the grating reflectivity, V is the visibility of the signals, $\Phi = 2\pi OPD/\lambda_B$, where $OPD = n_{eff}\delta L$, and $\Phi(t)$ is a random phase-drift term. A sinusoidal strain-induced change in λ_B from the FBG, ($\delta\lambda_B$), induces a change in phase shift in Eq. (3), given by

$$\delta\Phi\sin\omega t = \left(2\pi OPD/\lambda_B\right)\left(\delta\lambda_B\right)\sin\omega t \tag{4}$$

Hence from Eq. (3), strain-induced changes in λ_B induce a corresponding phase modulation of the electrical carrier produced at the detector by the phase modulator, which we measured by determining

the amplitudes of the upper and lower sideband frequency components observed on an FFT spectrum analyser.

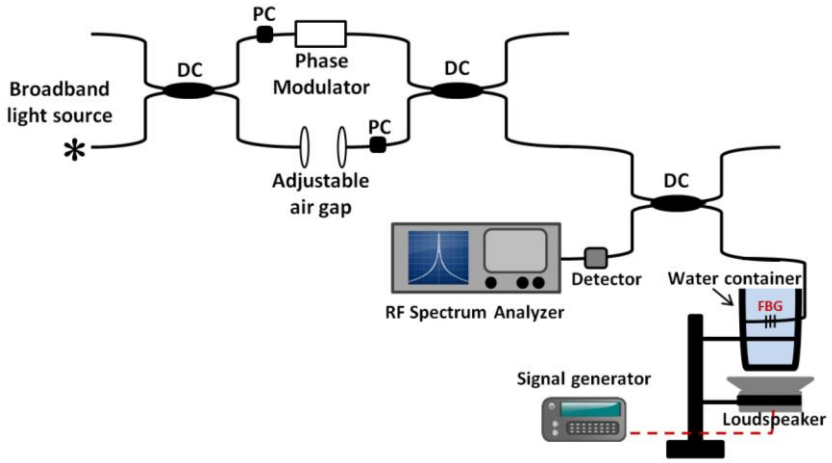

Figure 6. Experimental arrangement. DC: directional coupler, PC: polarization controller.

Two effects affect the sensitivity of the system. First, from Eq. (4), an increase in OPD results in a proportional increase in the amplitude of the phase modulation. Second, increasing the OPD beyond the coherence length of the light reflected by the FBG results in a reduction in the visibility and consequently the height of the carrier and sidebands. Therefore, the sensitivity was optimized by adjusting the OPD to achieve the maximum sideband amplitude. Initially, we calculated the OPD between the two arms of the designed MZI by recording the interference pattern on an OSA using the broadband source. Then, the length difference δL between the two arms of the MZI can be calculated by

$$\delta L = \frac{\lambda_B^2}{2\pi n_{eff}\delta\lambda_B}\delta\phi\,, \tag{5}$$

where $\delta\Phi$ is the phase difference, and $\delta\Phi = 2\pi$ for two adjacent peaks separated by the free spectral range.

When the fiber is compressed, the fractional change of the Bragg wavelength $\delta\lambda_B/\lambda_B$, in response to a pressure change δP, is given by [19]:

$$\frac{\delta\lambda_B}{\lambda_B} = \frac{\Delta\left(n_{eff}\Lambda\right)}{n_{eff}\Lambda} = \left[\frac{1}{\Lambda}\frac{\partial\Lambda}{\partial P} + \frac{1}{n_{eff}}\frac{\partial n_{eff}}{\partial P}\right]\delta P\,, \tag{6}$$

where Λ is the spatial period of the grating. The fractional change in physical length of the fiber and refractive index of the fiber core, respectively, are given by:

$$\frac{\delta L}{L} = -\frac{\left(1-2\upsilon\right)P}{E} \tag{7}$$

$$\frac{\delta n_{eff}}{n_{eff}} = \frac{n_{eff}^2 P}{2E}\left(1-2\upsilon\right)\left(2p_{12}+p_{11}\right) \tag{8}$$

where E and υ are the Young modulus and Poisson ratio of the fiber, respectively, and p_{11} and p_{12} are the components of the strain-optic tensor. As the fractional change in the spatial period of the grating equals the fractional change in the physical length of the sensing section, the pressure sensitivity is then expected to be

$$\frac{1}{\lambda_B}\frac{\delta\lambda_B}{\delta P} = -\frac{1}{E}\left((1-2\upsilon) - \frac{n_{eff}^2}{2}(1-2\upsilon)(2p_{12}+p_{11})\right) \tag{9}$$

With reference to equation (9), the first part in the parenthesis relates to the change in the period of the fabricated grating planes within the fiber core, whereas the second part relates to the refractive index change as a result of the strain optic effect. However, equation (9) is relevant for an isotropic solid, which is acceptable for silica optical fiber; conversely POF is not an isotropic material and so equation (9) may lack validity for POF. During the drawing process of POF manufacture the molecular polymer chains tend to align along the fiber axis, and are therefore an example of a transverse isotropic material where the properties perpendicular to the fiber axis are not the same as the properties that are along the fiber axis.

Using the values presented in Table 1 for the parameters E, υ, n_{eff}, p_{11} and p_{12} for silica and polymer fibers, the predicted fractional wavelength shift is -2.8x10^{-6} /MPa using silica fiber and -1.8x10^{-6} /MPa using polymer fiber, an improvement of around 1.5 times for homogenous PMMA fiber. In fact, in [72] the measured fractional changes were -2.5x10^{-6} /MPa (for silica fiber) and 83x10^{-6} /MPa (for POF), where these experimental results refer to some initial static pressure tests. Also, they showed that the wavelength shift with POF is opposite to that with silica (and much higher in magnitude). We could only explain that by allowing the fiber to be anisotropic as mentioned above.

From our experimental results and using the Bessel Function, the $V_{sideband}/V_{carrier}$ for POF and silica were 0.35 and 0.06, respectively, which means $V_{sideband}/V_{carrier} = J_1(\Phi)/ J_0(\Phi)$ where $J_0(\Phi)$ is approximately 1 for small phase modulations. So, after calculating the $J1(\Phi)$ for both cases, we achieved $J_1(\Phi)$ 0.17 for POF case, and 0.025 for silica fiber. With this signal processing scheme, the phase modulation we measured is directly proportional to the wavelength modulation experienced by the FBG. In fact, the amplitude of the wavelength modulation is given by $\lambda_B^2\Phi / 2\pi OPD$. So, the wavelength modulation for the POF is about 6 times greater than that for the silica. The significant difference between our results when compared with the work in [72] can be explained by our fiber perhaps being less anisotropic; typically the case if the fiber is drawn under lower stress.

Table 1: Material properties of PMMA and fused silica.

	PMMA	**Fused silica**
Parameter		
p_{11}	0.300	0.126
p_{12}	0.297	0.260
E (GPa)	2.95	72.45
n_{eff}	1.481	1.465
υ	0.370	0.165

The phase modulator was ramped, and hence generated a carrier signal, at 10 kHz. The silica and polymer FBGs had nominal Bragg wavelengths of 1550.21 nm and 1573.42 nm, with reflectivities of 90%

and 80%, respectively, and both FBGs had a bandwidth around 0.5 nm. Hence, in this scheme, acoustically induced changes in the wavelength reflected from FBG induce a phase modulation of the electrical carrier produced by the phase modulator, which we measured by determining the amplitudes of the side bands observed on the spectrum analyser. As shown in Fig. 6, a standard 8 Ω loudspeaker was driven in continuous mode by a signal generator tuned at the frequency 420 Hz to excite the FBG in water (and in air for comparison). Acoustic signals coming from the loudspeaker excites vibrations in the container where the FBG is attached, which in turn induces strain in the FBG sensor.

Fig. 7 (a) shows the 10 kHz carrier signal and sidebands observed on the spectrum analyser for 0.0625 and 25 W of acoustical power from the loudspeaker when the silica FBG is in air. Fig. 7 (b) shows the detected power of the sidebands (normalized with respect to the carrier signal power) as a function of the acoustical power. From Fig. 7 (b), the results demonstrate a highly linear response over the entire measurement region. The same analysis, but using the container with water, is shown in Figs. 8 (a) and (b). In this case, the difference between carrier amplitude and sidebands amplitude is reduced (25 dB) when compared with the case in air (29 dB). The signal-to-noise ratio measured by the spectrum analyser was 52 dB. Therefore, if the noise-limited resolution is defined as the RMS pressure amplitude that would lead to a signal-to-noise ratio of unity, the resolution may be calculated to be 3.68×10^{-5} Pa within a 100 Hz bandwidth, corresponding to 3.68×10^{-6} Pa/Hz$^{1/2}$.

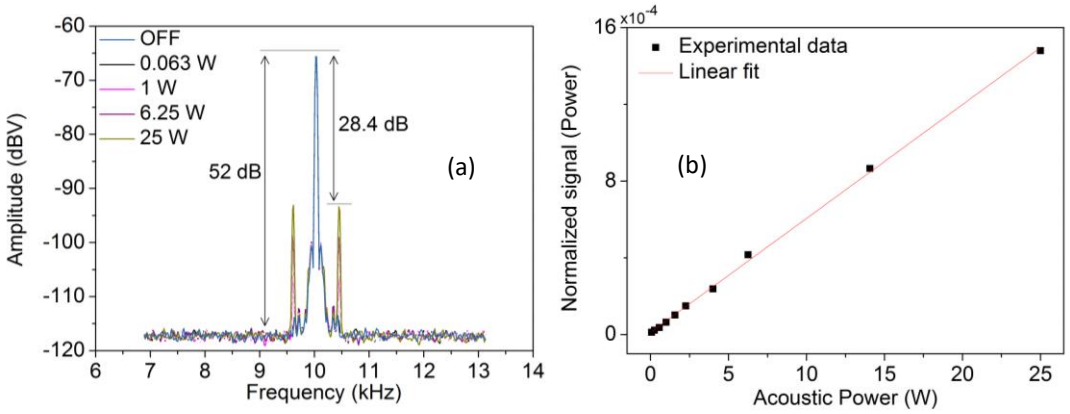

Figure 7. (a) The carrier signal at 10 kHz and sidebands for different acoustical powers when the silica FBG sensor is in air. (b) The side-band power (normalized with respect to the carrier power) as a function of the acoustical power.

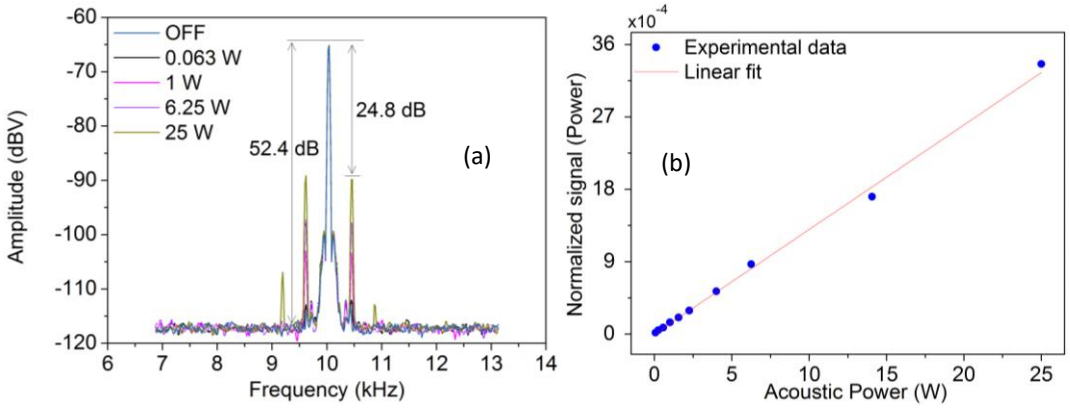

Figure 8. (a) The carrier signal at 10 kHz and sidebands for different acoustical powers when the silica FBG sensor is in water. (b) The side-band power (normalized with respect to the carrier power) as a function of the acoustical power.

Tests were conducted when a POFBG is used instead of silica FBG. The previous conditions presented for silica FBG are kept to compare the performance. Fig. 9 shows the 10 kHz carrier signal and sidebands observed on the spectrum analyser for no power from loudspeaker and for 25 W of acoustical when the POFBG is in air. In air, we can observe that the sideband's amplitude is weak at 25 W of acoustical power when compared with silica FBG sensor case. Fig. 10 (a) presents the carrier signal at 10 kHz and sidebands for acoustical power from 0.0625 to 25 W, when the container has the POFBG in water. Fig. 10 (b) illustrates the detected power of the sidebands (normalized with respect to the carrier signal power) as a function of the acoustical power. Here, the sidebands are strong compared with the air case, showing a high linear response. The difference between carrier and sidebands amplitude is reduced when compared with the case of a silica FBG sensor, achieving 9 dB of rejection, almost 3 times less than the silica FBG sensor in water. The signal-to-noise ratio measured by the spectrum analyser was 17 dB. To determine the noise-limited resolution of the system, the same procedure as above was used, and the result was 1.33×10^{-4} Pa/Hz$^{1/2}$.

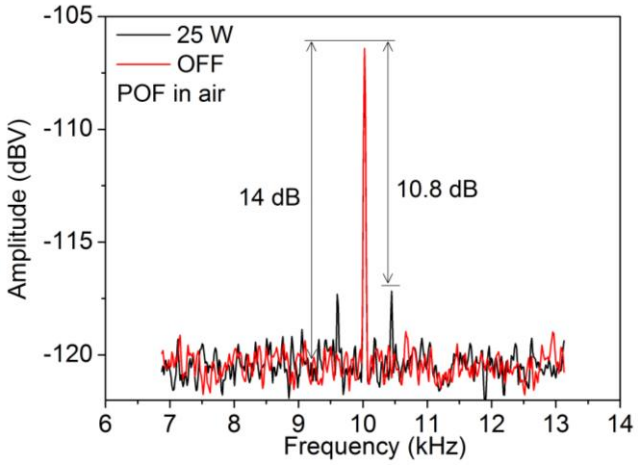

Figure 9. The carrier signal at 10 kHz and side bands for acoustical powers at 0 W (OFF) and 25 W when the POFBG sensor is in air.

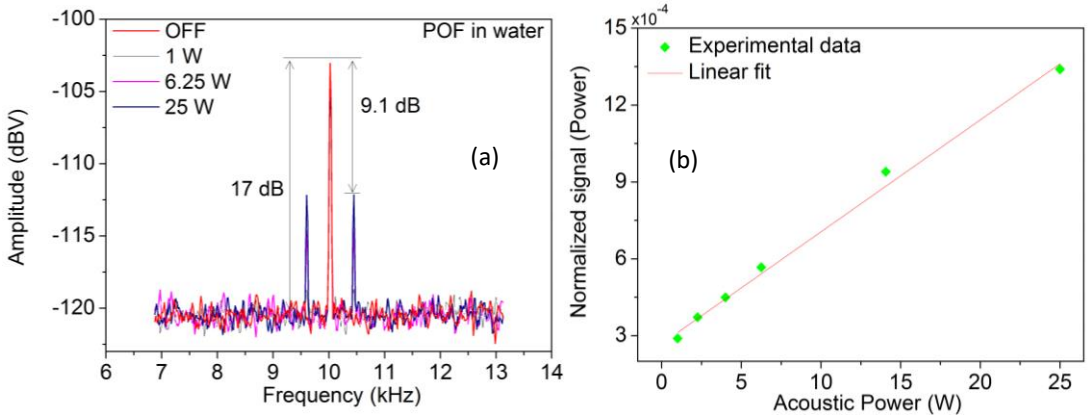

Figure 10. (a) The carrier signal at 10 kHz and side bands for different acoustical powers when the POFBG sensor is in water. (b) The side-band power (normalized with respect to the carrier power) as a function of the acoustical power.

In conclusion, we have presented our recent experimental results towards the development of a polymer FBG based sensor for underwater safety sensing. A FBG based sensor head and a fiber MZI have been fabricated for this purpose for monitoring low-frequency (few kHz) waves. A heterodyne technique based on an unbalanced interferometric wavelength discriminator is described and the performances of both types of fiber containing FBGs are compared. A considerable sensitivity improvement is achieved using polymer FBG (around 6 times better), which arises as a result of the much more compliant nature of POF compared to silica fiber. These results give us noise-limited pressure resolutions of 3.68×10^{-6} and 1.33×10^{-5} Pa/Hz$^{1/2}$ for silica and POF, respectively. Although POF presents more sensitivity than silica fiber, its resolution needs to be improved with the use of lower wavelengths or CYTOP fiber [24], which would allow us to considerably reduce the losses in the POF system.

4.2. Time-dependent variation of PMMA and TOPAS polymer FBG sensors in liquid level sensing

Research into liquid level sensing technologies is of great importance for human safety because such measurements are crucial to industrial applications such as fuel storage, for providing flood warning or tides and also in the biochemical industry. Many optical fiber liquid level sensors have been reported to be safe and reliable in different environments and present many advantages for liquid level measurement [7, 73-78], including for aircraft fuel level monitoring system [79]. However, most of these sensors have not been commercialized as an alternative to the traditional liquid level sensors because they exhibit some drawbacks, such as low sensitivity, limited range, long-term instability, limited resolution, high cost, or general weaknesses. The most frequently used level sensors are the capacitive and ultrasonic devices, however they suffer from intrinsic safety concerns in explosive environments combined with issues related with reliability and maintainability. Recently, we have presented new approaches for liquid level sensor systems [7,73,78] which may overcome these drawbacks but some studies need to be investigated and discussed about their time-dependent variation of the polymer FBGs' optical properties. So, these drawbacks presented above are solved where a new and robust approach was achieved [7,73,78] with high sensitivity, large range (from 0.8 m to a few meters depending on the diaphragm thickness), good resolution (less than 6 mm) and a relative low-cost when compared with the optical solutions already published [74-77]. Furthermore, these new approaches have several advantages: a) Fault tolerance: malfunctioning sensors can be identified and their outputs ignored; b) Operation is independent of the fuel density: changing the density alters the slope of the fitted line, but not its intercept; c) Operation is insensitive to g-force: this again changes the slope of the line but not its intercept; d) Temperature insensitivity: temperature induced shifts in both the nominal Bragg wavelengths of the sensors and the sensitivity of the sensors are compensated for. It should be noted that the aircraft fuel gauging problem is particularly demanding since not only can the effective g-force vary due to acceleration, but the attitude of the plane to the effective gravitational force can also change; it means, the plane of the liquid surface can have different orientations with respect to the airframe structure. This is a problem common to almost all gauging systems and it is solved by having multiple level gauges coupled with appropriate signal processing as demonstrated in [7].

Additionally, a preliminary study of the time-dependent variation of both the strength and resonance wavelength of polymer FBG array sensors is reported. The polymer FBGs are embedded in silicone rubber and polyurethane resin diaphragms and placed in contact with water and JET A-1 aircraft fuel, respectively [7]. Both the reflection and the resonance wavelength shift were monitored over time and two studies were made: first one, which in addition to the polymer FBG coated with the diaphragm also

the rest of the fiber is totally coated between the sensors with the same material; second one, in which the fiber between sensors is uncoated – in direct contact with liquid. Fig. 11 shows the experimental apparatus with sensors submerged in liquid: three sensors in fuel and five sensors in water. Note that fuel contains small amount of water and it can be detected by POF sensors as reported in [17]. More details about diaphragm fabrication and experimental setup can be found in [7,73].

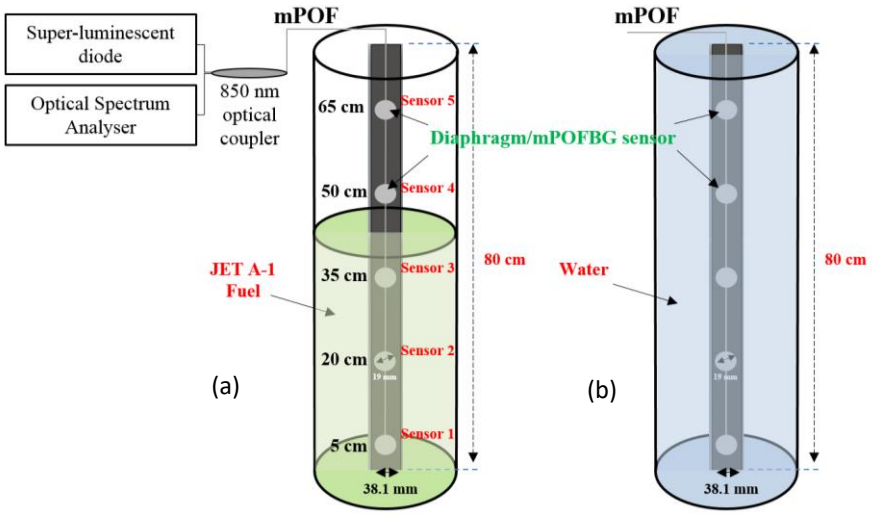

Figure 11. Experimental apparatus with sensors submerged in liquid: (a) three sensors in fuel and (b) five sensors in water.

PMMA and TOPAS FBGs were used, achieving for PMMA (after 90 days) short-term drifts (although the coated case showed very low changes, the equilibrium is not completely reached) for the first study mentioned above, and long-term drifts for the second case, possibly due to the sensitivity of PMMA to the water. Currently, we have studies in progress to evaluate the impact with more detail. On the other hand, TOPAS FBGs revealed a much improved behavior for long-term liquid monitoring systems suggesting a good option for this type of applications, as shown in Fig. 12.

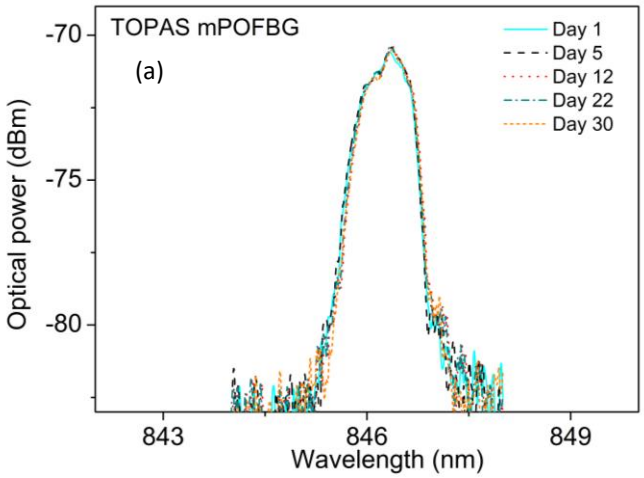

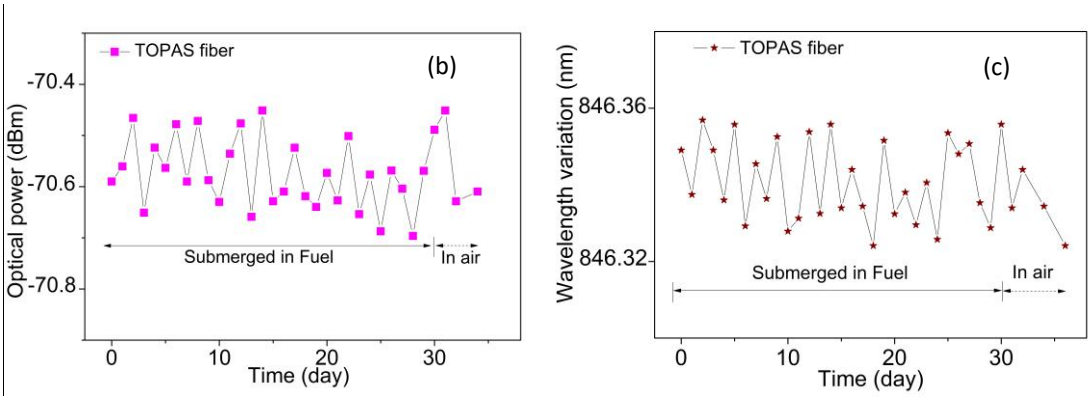

Figure 12. (a) Reflected spectra of the TOPAS mPOFBG over 30 days when the sensor is submerged in fuel. TOPAS mPOFBGs (b) reflection behavior and (c) resonance wavelength variation over the time for sensor.

5. Conclusion

The increased interest in POF technology is due to the different material properties compared to silica. This paper addresses the recent research and developments of POF sensor technology in different areas of human life safety, with focus on fiber Bragg grating based sensors and intensity variation schemes based sensors. The market is still demanding low-cost solutions where POF can play a relevant role more than ever. In conclusion, it is expected that POF based sensors will continue to be a very active research topic since there is an increasing number of research groups around the world currently focusing on the stabilization of this technology, tackling their problems.

Acknowledgments

This work was supported by Fundação para a Ciência e Tecnologia (FCT)/MEC through national funds and when applicable co-funded by FEDER – PT2020 partnership agreement under the projects UID/EEA/50008/2013, and UID/CTM/50025/2013. C. A. F. Marques also acknowledges the financial support from FCT through the fellowship SFRH/BPD/109458/2015. The research leading to these results has also received funding from the Marie Curie Actions of the European Union's 7th Framework Programme FP7/2007-2013/ under REA grant agreement No. 608382. The authors are grateful to Prof. O. Bang and Dr. D. Sáez-Rodríguez for providing some fibers used in this work.

References

[1] D. J. Webb, "Fibre Bragg grating sensors in polymer optical fibres", Measurement Science and Technology 26, 092004 (2015).
[2] F. Bischoff, "Organic polymer biocompatibility and toxicology", Clinical chemistry 18, 869 (1972).
[3] M.C.J. Large, J. Moran, L. Ye, "The role of viscoelastic properties in strain testing using microstructured polymer optical fibres (mPOF)", Measurement Science and Technology 20, 034014 (2009).
[4] J. G. A. Griffiths, Tables of physical and chemical constants. By G. W. C. Kaye and T. H. Laby. The Analyst 73 (1948) 704.
[5] S. Kiesel, P. Van Vickle, K. Peters, T. Hassan, M. Kowalsky, "Intrinsic polymer optical fiber sensors for high-strain applications", in: D. Inaudi, W. Ecke, B. Culshaw, K. J. Peters, E. Udd, (Eds.), 616713-616713-11 (2006).
[6] X. Hu, D. Sáez-Rodríguez, C. A. F. Marques, O. Bang, D. J. Webb, P. Mégret, C. Caucheteur, "Polarization effects in polymer FBGs: study and use for transverse force sensing," Opt. Express 23, 4581 (2015).
[7] C. A. F. Marques, A. Pospori, D. Sáez-Rodríguez, K. Nielsen, O. Bang, D.J. Webb, Aviation Fuel Gauging Sensor Utilizing Multiple Diaphragm Sensors Incorporating Polymer Optical Fiber Bragg Gratings. IEEE Sensors Journal 16, 6122 (2016).

[8] C. Broadway, D. Gallego, A. Pospori, M. Zubel, D. J. Webb, K. Sugden, G. Carpintero, H. Lamela, "Microstructured polymer optical fibre sensors for opto-acoustic endoscopy", Proc. SPIE 9886, Micro-Structured and Specialty Optical Fibres IV, 98860S-6 (2016).
[9] W. Zhang, D.J. Webb, G.D. Peng, "Investigation Into Time Response of Polymer Fiber Bragg Grating Based Humidity Sensors", Journal of Lightwave Technology 30, 1090 (2012).
[10] W. Yuan, L. Khan, D. J. Webb, K. Kalli, H. K. Rasmussen, A. Stefani, O. Bang, "Humidity insensitive TOPAS polymer fiber Bragg grating sensor," Opt. Express 19, 19731 (2011).
[11] G. Woyessa, A. Fasano, A. Stefani, C. Markos, K. Nielsen, H. K. Rasmussen, O. Bang, "Single mode step-index polymer optical fiber for humidity insensitive high temperature fiber Bragg grating sensors," Opt. Express 24, 1253 (2016).
[12] S. Ando, T. Matsuura, S. Sasaki, "Perfluorinated polymers for optical waveguides", Chemtech 24, 20 (1994).
[13] A. Abang, and D.J. Webb, "Effects of annealing, pre-tension and mounting on the hysteresis of polymer strain sensors", Measurement Science and Technology 25, 015102 (2014).
[14] G. A. Cranch, R. Crickmore, C. K. Kirkendall, A. Bautista, K. Daley, S. Motley, J. Salzano, J. Latchem, P. J. Nash, "Acoustic performance of a large-aperture, seabed, fiber-optic hydrophone array", Journal of the Acoustical Society of America 115, 2848 (2004).
[15] P. J. Nash, G. A. Cranch, D. J. Hill, "Large scale multiplexed fibre-optic arrays for geophysical applications", Proceedings of the Society of Photo-Optical Instrumentation Engineers (SPIE) 42022000, 55 (2000).
[16] E. Mesquita, T. Paixão, P. Antunes, F. Coelho, P. Ferreira, P.S André, H. Varum, "Groundwater level monitoring using a plastic optical fiber", Sensors and Actuators A-Physical, 240, 138 (2016).
[17] W. Zhang, D. J. Webb, M. Carpenter, C. Williams, "Measuring water activity of aviation fuel using a polymer optical fiber Bragg grating". 23rd international conference on Optical Fibre Sensors. SPIE, 2014. 91574V (Proceedings of SPIE; Vol. 9157).
[18] O. R. Costilla, P. Scully, K. Ozanyan, "Temporal Pattern Recognition in Gait Activities Recorded with a Footprint Imaging Sensor System", IEEE Sensors Journal, PP (99), (2016) 10.1109/JSEN.2016.2583260
[19] D. Gallego and H. Lamela, "High-sensitivity ultrasound interferometric single-mode polymer optical fiber sensors for biomedical applications," Opt. Lett. 34, 1807 (2009).
[20] C. Leitão, P. Antunes, J. L. Pinto, J. Bastos, P. S. André, "Carotid distension waves acquired with a fiber sensor as an alternative to tonometry for central arterial systolic pressure assessment in young subjects", Measurement 95, 45 (2017).
[21] P. Stajanca, K. Krebber, "Radiation induced attenuation in perfluorinated polymer optical fibres for dosimetry applications", POF 2016, Birmingham, (2016). ISBN 978 1 85449 408 5.
[22] P. Antunes, J. M. S. Dias, H Varum, P.S André, "Dynamic structural health monitoring of a civil engineering structure with a POF accelerometer", Sensor Review 34, 36 (2014).
[23] B. M. Quandt, L. J. Scherer, L. F. Boesel, M. Wolf, G.-L. Bona, R. M., Rossi, "Body-Monitoring and Health Supervision by Means of Optical Fiber-Based Sensing Systems in Medical Textiles", Adv. Healthcare Mater. 4, 330 (2015).
[24] A. Lacraz, M. Polis, A. Theodosiou, C. Koutsides, K. Kalli, "Femtosecond laser inscribed Bragg gratings in low loss CYTOP polymer optical fibre" IEEE Phot. Techn. Letters 27, 693 (2015).
[25] C. Markos, A. Stefani, K. Nielsen, H. K. Rasmussen, W. Yuan, O. Bang, "High-Tg TOPAS microstructuredpolymer optical fiber for fiber Bragg grating strain sensing at 110 degrees," Opt. Express 21, 4758 (2013).
[26] A. Fasano, G. Woyessa, P. Stajanca, C. Markos, A. Stefani, K. Nielsen, H. K. Rasmussen, K. Krebber, O. Bang, "Fabrication and characterization of polycarbonate microstructured polymer optical fibers for high-temperature-resistant fiber Bragg grating strain sensors," Opt. Mater. Express 6, 649 (2016).
[27] K. E. Carroll, C. Zhang, D. J. Webb, K. Kalli, A. Argyros, M. C. J. Large, "Thermal response of Bragg gratings in PMMA microstructured optical fibers," Opt. Express 15, 8844 (2007).
[28] C. Zhang, W. Zhang, D. J. Webb, G. D. Peng, "Optical fibre temperature and humidity sensor," Electron. Lett. 46, 643 (2010).
[29] W. Yuan, A. Stefani, M. Bache, T. Jacobsen, B. Rose, N. Herholdt-Rasmussen, F. K. Nielsen, S. Andresen, O. B. Sørensen, K. S. Hansen, O. Bang, "Improved thermal and strain performance of annealed polymer optical fiber Bragg gratings," Opt. Commun. 284, 176 (2011).
[30] W. Yuan, A. Stefani, O. Bang, "Tunable polymer Fiber Bragg Grating (FBG) inscription: Fabrication of dual-FBG temperature compensated polymer optical fiber strain sensors," IEEE Photon. Technol. Lett. 24, 401 (2012).
[31] I. P. Johnson, D. J. Webb, K. Kalli, M. C. J. Large, A. Argyros, "Multiplexed FBG sensor recorded in multimode microstructured polymer optical fibre," Proc. SPIE 7714, 77140D-10 (2010).
[32] A. Cusano, A. Cutolo, and J. Albert, "Fiber Bragg Grating Sensors: Recent Advancements", Industrial Applications and Market Exploitation (Bentham Science Publishers, 2009), Chap. 15.
[33] K. Makino, T. Kado, A. Inoue, Y. Koike, "Low loss graded index polymer optical fiber with high stability under damp heat conditions," Opt. Express 20, 12893 (2012).
[34] G. Emiliyanov, J. B. Jensen, O. Bang, P. E. Hoiby, L. H. Pedersen, E. M. Kjaer, L. Lindvold, "Localized biosensing with TOPAS microstructured polymer optical fiber," Opt. Lett. 32, 460 (2007).

[35] G. Emiliyanov, J. B. Jensen, O. Bang, P. E. Hoiby, L. H. Pedersen, E. M. Kjaer, L. Lindvold, “Localized biosensing with TOPAS microstructured polymer optical fiber: Erratum,” Opt. Lett. 32, 1059 (2007).
[36] G. Khanarian, “Optical properties of cyclic olefin copolymers,” Opt. Eng. 40, 1024 (2001).
[37] M. Koerdt, S. Kibben, J. Hesselbach, C. Brauner, A. S. Herrmann, F. Vollertsen, L. Kroll, "Fabrication and characterization of Bragg gratings in a graded-index perfluorinated polymer optical fiber", 2nd Int. Conf. on System-Integrated Intelligence: Challenges for Product and Production Engineering Procedia Technol. 15 138, (2014).
[38] Y. Koike, T. Ishigure, E. Nihei, “High-Bandwidth Graded-Index Polymer Optical Fiber,” J. Lightwave Technol. 13, 1475 (1995).
[39] A. Tanaka, H. Sawada, T. Takoshima, N. Wakatsuki, “New plastic optical fiber using polycarbonate core and fluorescence-doped fiber for high temperature use,” Fiber Integr. Opt. 7, 139 (1988).
[40] S. Irie and M. Nishiguchi, “Development of the heat resistant plastic optical fiber,” in Proceedings of the Third International Conference on Plastic Optical Fibres & Applications, (Yokohama, Japan), 88 (1994).
[41] O. Ziemman, J. Krauser, P. E. Zamzow, W. Daum, "POF Handbook. Optical Short Range Transmission Systems" (Springer, 2008), Chap. 2 (2008).
[42] D. G. Legrand and J. T. Bendler, Handbook of Polycarbonate Science and Technology (Marcel Dekker, 2000).
[43] Bayer Material Science AG, “Optical properties of Makrolon and Apec for non-imaging optics,” (Bayer Material Science AG, 2014).
[44] P. Roriz, O. Frazão, A. B. Lobo-Ribeiro, J. L. Santos, "Review of fiber-optic pressure sensors for biomedical and biomechanical applications", J. Biomed. Opt. 18, 050903 (2013).
[45] A. Othonos, "Fiber Bragg gratings", Rev. Sci. Instrum. 68, 4309 (1997).
[46] R. Kashyap, Fiber Bragg Grating, Academic Press, New York (1999).
[47] T. Erdogan, “Fiber grating spectra,” J. Lightwave Technol. 15, 1277 (1997).
[48] T. Erdogan, J. E. Sipe, “Tilted Fiber Phase Gratings,” Opt. Soc. Am. A 13, 296 (1996).
[49] A. Othonos, K. Kalli, Fiber Bragg Gratings: Fundamentals and Applications (Artech House, 1999).
[50] C. A. F. Marques, L. Bilro, N. J. Alberto, D. J. Webb, R. N. Nogueira, “Narrow bandwidth Bragg gratings imprinted in polymer optical fibers for different spectral windows,” Opt. Commun. 307, 57 (2013).
[51] X. Hu, C.-F. J. Pun, H.-Y. Tam, P. Mégret, C. Caucheteur, “Tilted Bragg gratings in step-index polymer optical fiber”, Opt. Lett. 39, 6835 (2014).
[52] X. Hu, P. Mégret, C. Caucheteur, “Surface Plasmon excitation at near-infrared wavelengths in polymer optical fibers”, Opt. Lett. 40, 3998 (2015).
[53] C. A. F. Marques, P. Antunes, P. Mergo, D. J. Webb, P. André, "Chirped Bragg gratings in PMMA step-index polymer optical fiber", IEEE Photon. Technol. Lett. 29, 500 (2017).
[54] K. S. Feder, P. S. Westbrook, J. Ging, P. I. Reyes, G. E. Carver, “In-fiber spectrometer using tilted fiber gratings,” IEEE Photon. Technol. Lett. 15, 933 (2003).
[55] J. Peupelmann, J. Peupelmann, E. Krause, A. Bandemer, C. Schäffer, “Fibre-polarimeter based on grating taps,” IEEE Electron. Lett. 38, 1248 (2002).
[56] S. J. Mihailov, R. B. Walker, T. J. Stocki, D. C. Johnson, “Fabrication of tilted fibre-grating polarisation-dependent loss equaliser,” IEEE Electron. Lett. 37, 284 (2001).
[57] J. Albert, L.-Y. Shao, C. Caucheteur, “Tilted fiber Bragg grating sensors,” Laser & Photon. Rev. 7, 83 (2013).
[58] K. C. Byron, K. Sugden, T. Bricheno, I. Bennion, "Fabrication of chirped Bragg gratings in photosensitive fibre", Elect. Letters 29, 1659 (1993).
[59] F. Ouellette, “Dispersion cancellation using linearly chirped Bragg grating filters in optical waveguides,” Opt. Lett. 12, 847 (1987).
[60] B. J. Eggleton, A. Ahuja, P. S. Westbrook, J. A. Rogers, P. Kuo, T. N. Nielsen, B. Mikkelsen, "Integrated Tunable Fiber Gratings for Dispersion Management in High-Bit Rate Systems," J. Lightwave Technol. 18, 1418 (2000).
[61] A. Sun, Z. Wu, "A Hybrid LPG/CFBG for Highly Sensitive Refractive Index Measurements", Sensors 12, 7318 (2012).
[62] D. Tosi, E. G. Macchi, M. Gallati, G. Braschi, A. Cigada, S. Rossi, G. Leen, E. Lewis, "Fiber-optic chirped FBG for distributed thermal monitoring of ex-vivo radiofrequency ablation of liver," Biomed. Opt. Express 5, 1799 (2014).
[63] S. Yashiro, T. Okabe, N. Toyama, N. Takeda, "Monitoring damage in holed CFRP laminates using embedded chirped FBG sensors", International Journal of Solids and Structures 44, 603(2007).
[64] P. J. Scully, O. Costilla-Reyes, N. Ahmed, J. Vaughan, E. Stanmore, K. Ozanyan, " POF Sensing Grid: Signal Analysis to extract Human Motion Characteristics", POF 2016, Birmingham, (2016). ISBN 978 1 85449 408 5.
[65] H. U. Hassan, J. Janting, S. Aasmul, O. Bang, "Polymer Optical Fiber Compound Parabolic Concentrator fiber tip based glucose sensor: in-Vitro Testing," IEEE Sensors Journal 16, 8483 (2016).
[66] World Health Organization, “Diabete sFact Sheet”, June (2016) http://www.who.int/mediacentre/factsheets/fs312/en/
[67] G. A. Cranch, G. A. Miller, C. K. Kirkendall, “Fiber laser sensors: Enabling the next generation of miniaturized, wideband marine sensors”, Proceedings of Fiber Optic Sensors and Applications VIII (SPIE) 8028 (2011).

[68] M. Moccia, M. Consales, A. Iadicicco, M. Pisco, A. Cutolo, V. Galdi, A. Cusano, “Resonant Hydrophones Based on Coated Fiber Bragg Gratings,” IEEE/OSA J. Lightwave Technol. 30, 2472 (2012).
[769] A. Stefani, S. Andresen, W. Yuan, O. Bang, “Dynamic Characterization of Polymer Optical Fibers”, IEEE J. Sensors 12, 3047 (2012).
[70] C. A. F. Marques, L. Bilro, L. Kahn, R. A. Oliveira, D. J. Webb, R. N. Nogueira, “Acousto-Optic effect in microstructured polymer fiber Bragg gratings: simulation and experimental overview”, IEEE/OSA J. Lightw. Technol. 31, 1551 (2013).
[71] N. E. Fisher, D. J. Webb, C. N. Pannell, D. A. Jackson, L. R. Gavrilov, J. W. Hand, L. Zhang, I. Bennion, "Ultrasonic hydrophone based on short in-fiber Bragg gratings," Appl. Opt. 37, 8120 (1998).
[72] I. P. Johnson, D.J. Webb, K. Kalli, “Hydrostatic pressure sensing using a polymer optical fibre Bragg gratings”, Proc. of SPIE Vol. 8351 - 3rd Asia Pacific Optical Sensors Conference, 835106 (2012).
[73] C. A. F. Marques, G. D. Peng, David J. Webb, “Highly sensitive liquid level monitoring system utilizing polymer fiber Bragg gratings,” Opt. Express 23, 6058 (2015).
[74] G. Betta, L. Ippolito, A. Pietrosanto, A. Scaglione, “Optical fiber-based technique for continuous-level sensing,” IEEE Transactions on Instrumentation and Measurement 44, 686 (1995).
[75] T. Guo, Q. D. Zhao, Q. Y. Dou, H. Zhang, L. F. Xue, G. L. Huang, X. Y. Dong, “Temperature-insensitive fiber Bragg grating liquid-level sensor based on bending cantilever beam,” IEEE Photon. Technol. Lett. 17, 2400 (2005).
[76] C. B. Mou, K. M. Zhou, Z. J. Yan, H. Y. Fu, and L. Zhang, “Liquid level sensor based on an excessively tilted fiber grating,” Opt. Commun. 305, 271 (2013).[77] D. Sengupta, P. Kishore, “Continuous liquid level monitoring sensor system using fiber Bragg grating,” Opt. Eng. 53, 017102 (2014).
[78] C. A. F. Marques, A. Pospori, D. Sáez-Rodríguez, K. Nielsen, O. Bang, D. J. Webb, "Fiber optic liquid level monitoring system using microstructured polymer fiber Bragg grating array sensors: performance analysis", Proc. SPIE 9634, 24th International Conference on Optical Fibre Sensors, 96345V (2015).
[79] R. Langton, C. Clark, M. Hewitt, L. Richards, “Aircraft Fuel Systems”, Chichester, John Wiley & Sons, United Kingdom, (2009).